Ultrasound in Med. & Biol., Vol. 42, No. 11, pp. 2650–2661, 2016

0301-5629/$ - see front matter

http://dx.doi.org/10.1016/j.ultrasmedbio.2016.07.013

● *Original Contribution*

EXAMINATION OF EFFECTS OF LOW-FREQUENCY ULTRASOUND ON SCLERAL PERMEABILITY AND COLLAGEN NETWORK

Wai-Leung Langston Suen,* Jun Jiang,† Hoi Sang Wong,* Jianan Qu,† and Ying Chau*‡

*Department of Chemical and Biomolecular Engineering, Hong Kong University of Science and Technology, Hong Kong, China; †Department of Electronic and Computer Engineering, Hong Kong University of Science and Technology, Hong Kong, China; and ‡Division of Biomedical Engineering, Hong Kong University of Science and Technology, Hong Kong, China

(*Received* 2 *September* 2015; *revised* 23 *June* 2016; *in final form* 13 *July* 2016)

Abstract—Delivery of therapeutics to the intraocular space or to targeted tissues in the posterior segment is challenging because of the structural and dynamic barriers surrounding the eye. Previously, we reported the feasibility of using ultrasound (US) irradiation to deliver macromolecules to the posterior segment of the eye *via* the transscleral route, which consists of sclera as the outermost anatomic barrier. In this study, we found that although ultrasound increases scleral permeability for macromolecules, the scleral collagen arrangement remains undisturbed. In an *ex vivo* experiment, protein permeation across the sclera was significantly enhanced by ultrasound in the stable cavitation regime. The scleral collagen network was further examined by second harmonic generation imaging. Quantitative image analysis techniques were adopted to examine the density, anisotropy and interlacing pattern of collagen fibers before and after ultrasound irradiation. Repeated ultrasound applications did not induce significant changes in the arrangement of collagen fibrils at 40 kHz with a spatial average temporal average intensity (I_{SATA}) <1.8 W/cm^2. These parameters correspond to a mechanical index (MI) below 0.8 in our setting. These data suggested that enhanced permeation of macromolecules across the sclera was achieved without disturbing the collagen network of the sclera. This evidence supports that low-frequency, low-intensity ultrasound is a tolerable approach to transscleral drug delivery. (E-mail: ying.chau@ust.hk) © **2016 World Federation for Ultrasound in Medicine & Biology.**

Key Words: **Second harmonic generation imaging, Drug delivery, Mechanical index, Texture analysis, Collagen, Scleral permeability.**

INTRODUCTION

Transscleral delivery of high-molecular-weight compounds is an emerging technique for the delivery of therapeutic molecules for treatment of eye diseases (Ambati and Adamis 2002; Ambati et al. 2000; Geroski and Edelhauser, 2001; Thrimawithana et al. 2011). The outmost barrier in the transscleral route is the sclera. It has a large and accessible surface area and is proximal to the retina. However, the permeability of the sclera to macromolecules is quite low because of the dense network arrangement of acellular collagen fibrils interlinked with proteoglycans (Young 1985). The outward bulk fluid flow arising from osmotic and hydrostatic pressure further decreases the amount of drug molecules that can be effectively delivered (Kim et al. 2007). Hence, there is a need to increase the transscleral flux to overcome the aforementioned static barriers and dynamic clearance to enhance the transport of macromolecules into the intraocular space.

Our group recently discovered that, with the application of low-frequency, low-intensity ultrasound, transscleral delivery of macromolecules to the posterior segment of the eye was significantly enhanced in live rabbits. In that study, 40-kHz ultrasound was applied three times to the sclera of a live rabbit at an intensity I_{SATA} (spatial average temporal average intensity) of 0.12 W/cm^2 with a mechanical index (MI) of 0.20. Permeability of macromolecules across the sclera was returned to normal 2 wk after ultrasound irradiation. No damage to the ocular tissues was observed, and the visual function of the rabbits was not affected (Suen et al. 2013). In the study described here, our aim was to investigate the effect of ultrasound on the sclera. Answering this question leads to an understanding of ultrasound-enhanced transscleral transport by first focusing on the sclera. Bovine serum

Address correspondence to: Ying Chau, Hong Kong University of Science and Technology, Room 4353, Academic Building, Clear Water Bay, Kowloon, Hong Kong, China. E-mail: ying.chau@ust.hk

albumin protein was used in this study to evaluate transscleral transport enhancement postsonication. We hypothesized that ultrasound increases the permeability of the sclera. The effect of scleral permeability enhancement after ultrasound applications was evaluated at an I_{SATA} (spatial average and temporal average intensity) ranging from 0.002 to 1.8 W/cm^2. The selected intensity range covers both the stable cavitation regime and transient cavitation regime, which is equivalent to the range of the MI of ultrasound from 0.03 to 0.8 (Holland and Apfel 1989). The MI is a measure of the extent of cavitation and can be categorized into two regimes: stable cavitation (MI = 0.03–0.20), in which there is gentle periodic pulsation of cavities, and transient cavitation (MI $\geq$ 0.8), in which there occur vigorous pulsation and collapse of the cavities and the violent collapse of cavities that creates microjets. We further hypothesized that acoustic cavitation is essential for enhanced transscleral transport. Thus, protein penetration into the sclera after ultrasound application was measured at different MIs to determine if there was any correlation. If all these hypotheses held, it would remain to be determined whether the enhancement was related to changes in collagen fiber arrangement. This explanation could be challenged because micron-size pores within collagen network should not restrict the movement of macromolecules (Chopra et al. 2010). Also, concern over safety arises if the scleral collagen network is permanently altered as it is important for maintaining the shape of the eyeball and, therefore, visual function. The sclera helps to maintain the overall architecture of the eyeball (Ethier et al. 2004). Changes in the elastic properties of the sclera have been reported to impair vision (Watson and Young 2004). Another possible explanation for the improved scleral permeability would be changes in non-collagen constituents of scleral tissue (Young 1985). Proteoglycans, for example, influence hydration, solute diffusion, and fluid movement through the sclera, both from the uvea and *via* the trabecular meshwork (Watson and Young 2004). Modulation of the proteoglycan arrangement in the scleral matrix might also influence transscleral transport. Owing to the features of the imaging techniques, we focused on the effect of ultrasound on the scleral collagen fiber network in this study.

Second harmonic generation (SHG) imaging was employed to visualize the collagen fibril network. SHG imaging is a non-linear optical imaging technique. It is excellent for intrinsic 3-D image sectioning, producing high contrast superior to that of traditional linear optical imaging methods, such as confocal microscopy (Denk et al. 1990). Although SHG imaging does not exceed SEM (scanning electron microscopy) and AFM (atomic force microscopy) in terms of image resolution, it can be used to examine specimens non-invasively. Collagen has a highly crystalline triple-helix structure that is not centrosymmetric. This unique feature makes collagen a very effective "upconverter" of light for visualization by SHG, with a hyperpolarizability just 10-fold less than that of crystalline quartz (Fine and Hansen 1971; Han et al. 2005). Image texture analysis was conducted to quantitatively evaluate changes in the collagen network after ultrasound irradiation, including the density, alignment direction and interlacing pattern of the collagen network. These changes were measured by entropy analysis, GLCM analysis and Fourier transform analysis, respectively.

METHODS

Materials

Fluorescein isothiocyanate-labeled bovine serum albumin (FITC-BSA) (molecular weight: 65 kDa; Sigma, St. Louis, MO, USA) was used as the *ex vivo* drug model. FITC-BSA was selected because its molecular weight is comparable to the molecular weight of ranibizumab (Lucentis, molecular weight: 48 kDa) (Schmucker et al. 2010). FITC-BSA was dissolved in phosphate-buffered saline (PBS) solution to a final concentration of 0.1 wt % and is denoted as "BSA solution" hereinafter. The solution was light protected until the fluorescein measurement to reduce the photobleaching effect.

Animals

All experimental and animal handling procedures were in accordance with the requirements of the Animals (Control of Experiments) Ordinance (Cap. 340) and all relevant legislation and Codes of Practice in Hong Kong, All procedures were approved by the Faculty Committee on the Use of Live Animals in Teaching and Research at Hong Kong University of Science and Technology (APCF 2012010).

Ultrasound device and calibration

A 40-kHz ultrasound transducer (Beijing Cheng-Cheng Weiye Science and Technology, Beijing, China) was powered by a function generator (GFG-8216 A, GW Instek, Montclair, CA, USA), which was connected to an amplifier (Model 7500 Amplifier; Krohn-Hite, Brockton, MA, USA) to emit ultrasound waves. The input signal was monitored by an oscilloscope (DS1002 B Oscilloscope; Tektronix, Beaverton, OR, USA), which was connected in parallel to the amplifier (Suen et al. 2013). The driving frequency (which is the same as the pulse repetition frequency of a continuous wave) was measured with a membrane hydrophone (HMB-0500, Onda, Sunnyvale, CA, USA), which was connected to the oscilloscope. The center frequency was confirmed to be 40 kHz. The ultrasound intensity was measured

using the hydrophone. The average intensity was calculated by measuring the pressure variation across the ultrasound radiation zone. Both the ultrasound transducer and the hydrophone were fixed on two separate metal rails. The rail on which the hydrophone was fixed was made movable in three perpendicular axis directions. Both the ultrasound transducer and the hydrophone were dipped into a tank of degassed water. The hydrophone was then moved to a position at which the pressure generated by the ultrasound wave was the greatest (denoted as the spatial peak position). The plane that is parallel to the ultrasound transducer surface at the spatial peak position was scanned at a 1 × 1-cm grid by the hydrophone under the "pressure-square integral" mode. The data obtained were filtered by omitting those values smaller than 0.25 of the spatial peak (National Council on Radiation Protection and Measurements [NCRP] 1983), and the intensity can be calculated with the equation

$$I_{\mathrm{SATA}} = \frac{\mathrm{prr}\ \Sigma^{\mathrm{n}}(\mathrm{Pi}^2 > 0.25\ \mathrm{Max}\ \mathrm{Pi}^2)}{n\rho c} \qquad (1)$$

where I_{SATA} is the spatial-average-temporal-average intensity (W/cm^2); prr is the pulse repetition rate (equal to the frequency of ultrasound for a continuous wave) (Hz); Max Pi^2 is the maximum pressure-square integral; Σ^nPi^2>0.25 Max Pi is the sum of all data within the matrix with a value greater than 0.25 Max Pi^2 (Pa^2·s); n is the number of data points greater than 0.25 Max Pi^2 times the size of the grid (1 × 1 cm in the sample calculation), or the effective radiation area (cm^2); ρ is the density of the medium (1000 kg/m^3 for water in the sample calculation); and c is the speed of sound in the medium (1482 m/s in the sample calculation).

The MI of ultrasound was calculated using the following equation (Szabo 2004) without derating as the hydrophone measurement and the experimental setup were both done in the water-base environment:

$$\mathrm{MI} = \frac{P_{\mathrm{r}}}{f_c^{1/2}} \qquad (2)$$

Here, P_{r} is the peak rarefactional pressure in megapascals, and f_c is the center frequency in megahertz. The peak rarefactional pressure was measured using a hydrophone and a conditioning amplifier (Brüel & Kjær, Denmark; Model 2691-A-0 S2, two-channel [single probe] Intensity Conditioning Amplifier).

Detection of cavitation by acoustic emission

The method of detection was similar to that described by Farny et al. (2009). Briefly, the ultrasound probe was connected to a cylindrical tube 14 mm in diameter and 15 mm in height made with silicone rubber. The tube was filled with degassed phosphate-buffered saline, and a single-element ultrasonic atomizing transducer of 1.70-MHz central frequency (Model S-UAT03 A, Sound Components, Hong Kong) was placed at the other end of the tube. The 40-kHz ultrasound probe acted as the transmitter, and the single element transducer as the receiver, which was connected to an oscilloscope (Model TDS1002 B, Tektronix, Beaverton, OR, USA) with a sampling rate of 1 Giga sample/s. The signal generated by the receiver in response to the ultrasound produced by the transmitter was recorded by the oscilloscope. The oscilloscope was set to fast Fourier transform (FFT) mode to display the frequency spectrum. The spectrum was obtained by averaging 128 data points over time using the "Averaging" function in the oscilloscope. The averaged linear frequency spectrum was first normalized to the maximum value, and the relative amplitude of the broadband noise signal to the fundamental signal was calculated to determine the presence of inertial cavitation activity.

Ex vivo *ultrasound experiments*

FITC-BSA penetration measurement. Fresh sclera from the posterior segment of the rabbit eye was mounted on a Franz diffusion cell with a contact area of 0.238 mm^2 at room temperature (20 ± 2°C). The orbital side was facing the donor chamber, and the uveal side was facing the receiver chamber. An ultrasound absorber was placed at the bottom of the receiver chamber (Fig. 1). Two milliliters of degassed BSA solution was placed in the donor chamber, and 4 mL of degassed phosphate-buffered saline was placed in the receiver chamber.

Continuous ultrasound wave at 40 kHz using the aforementioned system was applied 3 cm from the sclera at I_{SATA} = 0.002, 0.01, 0.05, 0.38 or 1.8 W/cm^2 for 30 s. The whole setup was covered with aluminum foil to

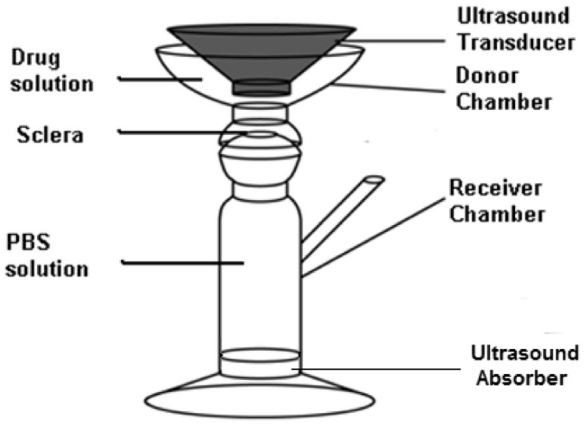

Fig. 1. Schematic of *ex vivo* ultrasound experiment setup. PBS = phosphate-buffered saline solution.

minimize the photobleaching of fluorescence materials. The sclera was in contact with BSA solution after ultrasound application for 15 min before cryosectioning. The surface temperature of the sclera was monitored before and after the ultrasound treatment using a thermocouple (206-3738, RS Components, Hong Kong). No ultrasound was applied in the control group.

Forty-eight pieces of sclera tissue were cryosectioned into 10-μm-thick sections using a cryostat (CM1850, Leica, Wetzlar, Germany). The sectioned tissues were viewed with a fluorescence microscope to determine the penetration distance of FITC-dextran (Cheung et al. 2010). Experiments under each condition were repeated at least three times ($n \geq 3$). The penetration distance of FITC-BSA across sclera was measured using ImageJ software. The measurements were taken perpendicular to the general orientation of the sclera. The penetration distance is defined as the distance from the sclera surface to the deepest depth at which the fluorescent signal reached the statistical threshold. The statistical threshold (*i.e.,* background signal of the slide) is defined as the average signal of the control sclera (not exposed to model drug). The same microscope setting and exposure time were used in capturing images from different experiments to obtain comparable contrast in the fluorescence images. The permeation distance was measured in three separate zones (zones are separated from each other by at least 100 μm) in each cryosectioned sclera sample. The arithmetical mean penetration distance of FITC-BSA in each intensity group was obtained from 12 sclera sections with a minimum of 20 measurements. Comparison between different conditions was performed by two-tailed *t*-test, and differences were considered statistically significant at $p < 0.05$.

Examination of scleral collagen arrangement. The setup was similar to that described above except that 2 mL of degassed phosphate-buffered saline solution was placed in the donor chamber. A continuous ultrasound wave at 40 kHz with $I_{SATA} = 0.002, 0.05, 0.12$ or 1.80 was applied 3 cm away to the sclera. The sclera was immediately removed from the setup for SHG imaging to determine the collagen fibril arrangement in the sclera.

Imaging experiment

An SHG microscope system was instrumented as described in previous work (Zeng et al. 2014). The excitation source was a femtosecond Ti:sapphire laser tuning at 740 nm. Two single-channel photomultiplier tubes connecting to a TCSPC board were used as the detection system, which covered two separate spectral bands: 370–400 nm and 500–700 nm. An actuator was used to control the imaging depth. Thirty consecutive images with the interval depth of 2 μm below the surface of sclera were collected for analysis in each site. In total, 48 pieces of sclera were used and were evenly divided into four groups according to the ultrasound parameter, that is, $I_{SATA} = 0.002, 0.05, 0.12$ and 1.8 W/cm^2. In each piece of sclera, six different sites were examined with the SHG microscope before and after insonation.

Image texture analysis. Three texture analyses techniques were used to quantitatively examine the changes in the sclera interfibrillar matrix, that is, the space between individual fibrils, the relative position of individual fibrils, the dominant orientation of the fibrils in a region and the interlacing pattern of the collagen network. All these methods captured the texture information of collagen fibrils on the XY image plane (parallel to the surface of the sclera) of each layer, which was obtained using the procedures illustrated in Figure 2 (Ferguson 2007). Briefly, after the 3-D image stacks are obtained from several different sites on the sclera, we first perform texture analysis on each layer and then average the data from all the layers in a stack. Finally, the data from different stacks are further averaged to obtain the final results for this sclera (this step is not illustrated in Fig. 2). In addition to the texture analysis, we created projection images for each 3-D stack using ImageJ software, which could provide a perspective view of the arrangement of collagen fibers (see Fig. 2).

Entropy analysis. Entropy was a first-order statistical description of texture. Entropy analysis was used to measure the texture randomness and determine the presence of collagen fibrils in an image; these were treated as random variables (Ihara 1993; Kuczynski and Mikolajczak 2003). Images with low entropy had little gray-level contrast. (An image that was perfectly flat has zero entropy.) On the other hand, images with high entropy had higher levels of contrast from one pixel to the next and were more "chaotic." In this study, the entropy of the 2-D image I was calculated using MATLAB software's built-in function; this was followed by taking the reciprocal of the value (1/entropy).

Fast Fourier transform (FFT_{AR}) analysis. Fourier analysis examines the texture in the frequency domain, and was regarded as a higher-order statistical analysis method. After the transformed image was obtained, texture information could be extracted to describe the morphology of the original image. Here, we focused on the orderliness of texture by calculating the asymmetry ratio: for a well-aligned pattern, its FFT image in the frequency domain would have higher values along the direction orthogonal to alignment. This would result in elliptic behavior in the respective intensity plot, indicating that the examined image has a high asymmetry ratio. On the contrary, the FFT image of an image with a random

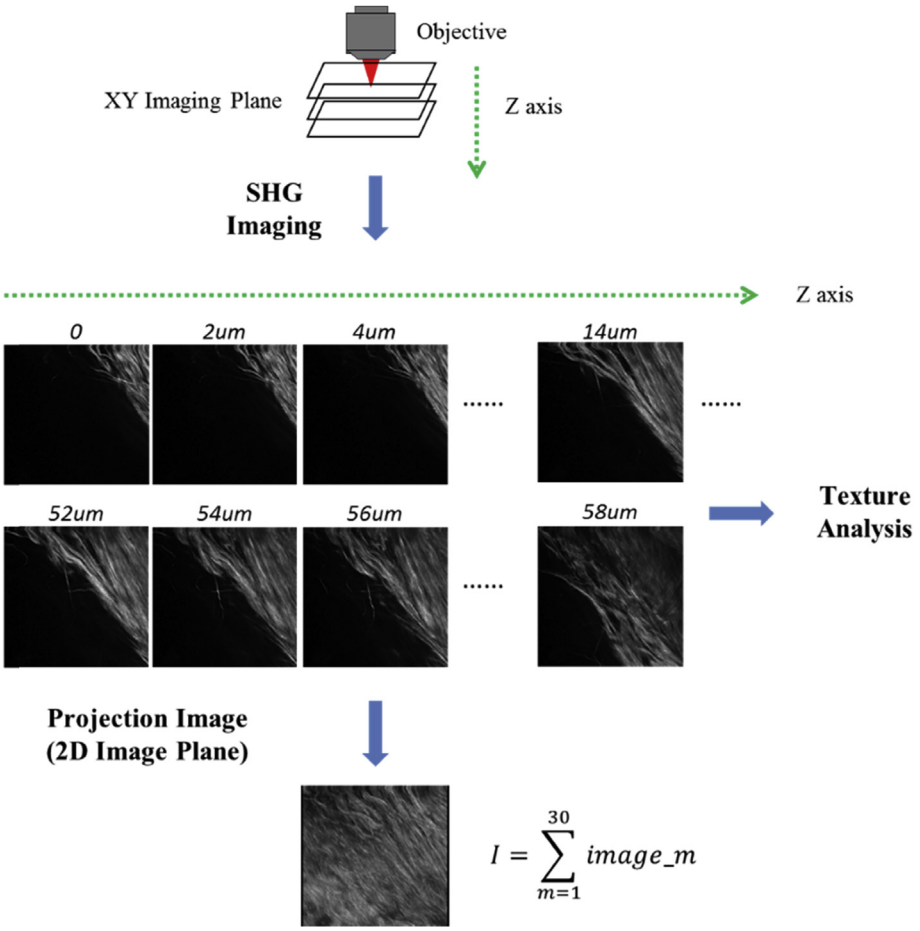

Fig. 2. Schematic of the image processing procedure. Texture analysis was performed on each layer, and then the values were averaged. The projection image here was actually obtained using ImageJ software and is equal to the sum all the images in a stack. SHG = second harmonic generation.

pattern would exhibit a circular plot, which indicates a low asymmetry ratio. The values of the asymmetric ratio of FFT (denoted as FFT_{AR}) images were obtained as the difference between the maximum and minimum of the line integral value (Zheng et al. 2011).

Gray-level co-occurrence matrix analysis. Gray-level co-occurrence matrix (GLCM) texture analysis was based on the second-order statistics (*i.e.,* statistics given by pairs of pixels) of gray-level pixel distribution (Haralick 1979; Zheng et al. 2011). The joint probability distribution of pairs of pixels (*i.e.,* how often a pixel with the gray-level value *i* occurs in a specific spatial relationship to a pixel with the value *j*) was defined as the GLCM, and different texture features could be deduced from the GLCM. In this study, we used GLCM correlation to evaluate the linear dependence between each pixel pair in the image. The higher value indicated that there were more similar structures in the image. Therefore, it could provide an estimate of the organization and structure of the collagen fibrils. Because GLCM was sensitive to direction and pixel distances, GLCM correlation was averaged from 0 to 180° and pixel distances from 1 to 48 in our analysis. The GLCM correlation was abbreviated $GLCM_{CORR}$ and was obtained from MATLAB codes (Haralick 1979).

Intraocular pressure measurement

The intraocular pressure of the eye of New Zealand white rabbits was recorded with Tonopen XL (Ametek, Berwyn, PA, USA) before and after application of 40-kHz ultrasound at the indicated intensities. Five samples were tested for each ultrasound intensity. Measurements with the Tonopen XL were repeated until the coefficient of variation was less than 5% (Lim et al. 2005).

RESULTS

Enhanced transscleral transport of macromolecules by ultrasound ex vivo

Penetration distance of FITC-BSA across *ex vivo* sclera was measured after application of 40-kHz

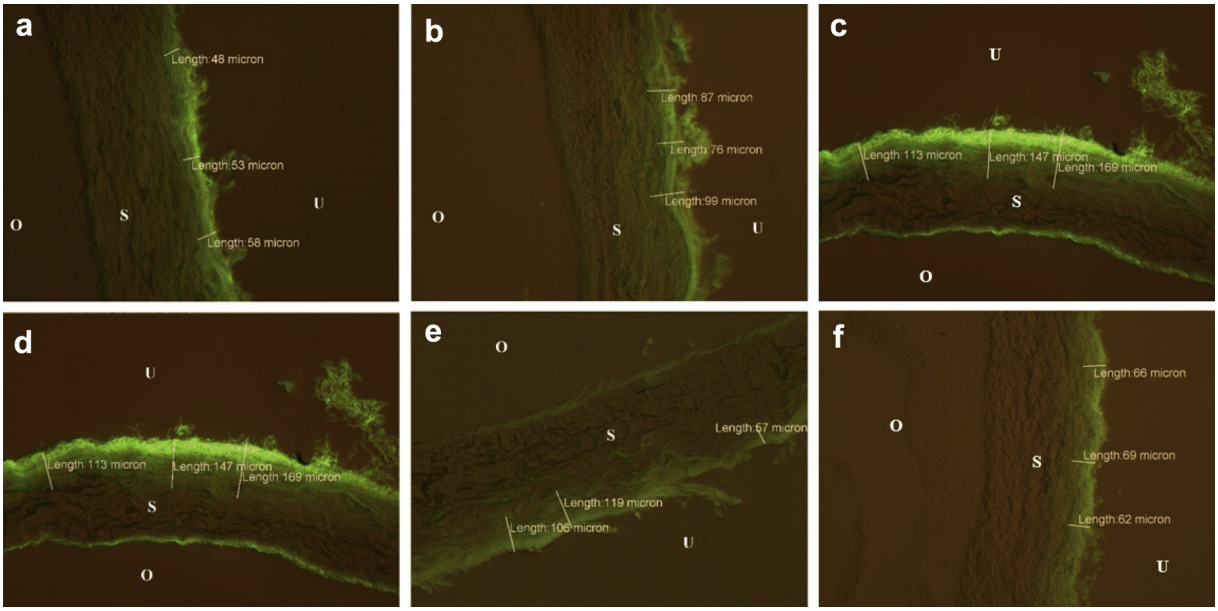

Fig. 3. Penetration of fluorescein isothiocyanate-labeled bovine serum albumin (FITC-BSA) after application of 40-kHz ultrasound for 30 s and 15 min of immersion: (a) control; (b) I_{SATA} = 0.002 W/cm^2; (c) I_{SATA} = 0.01 W/cm^2; (d) I_{SATA} = 0.05 W/cm^2; (e) I_{SATA} = 0.38 W/cm^2; (f) I_{SATA} = 1.8 W/cm^2; A representative cryosection viewed by fluorescence microscope is shown. U = uveal side; S = sclera; O = orbital side.

ultrasound at different intensities (Fig. 3). The bright-field and fluorescence images of cryosectioned sclera were combined before measurement of protein penetration distance using ImageJ software. The representative images of cryosectioned sclera and the measurement of penetration distance with ImageJ software are illustrated in Figure 3. The arithmetical mean thickness of the sclera is ~300 ± 32 μm; this value was obtained by averaging the thickness of 48 pieces of sclera tissue. The temperature on the surface of the sclera was measured before and after sonication. Negligible temperate changes (<0.1°C) were detected after the sclera was sonicated

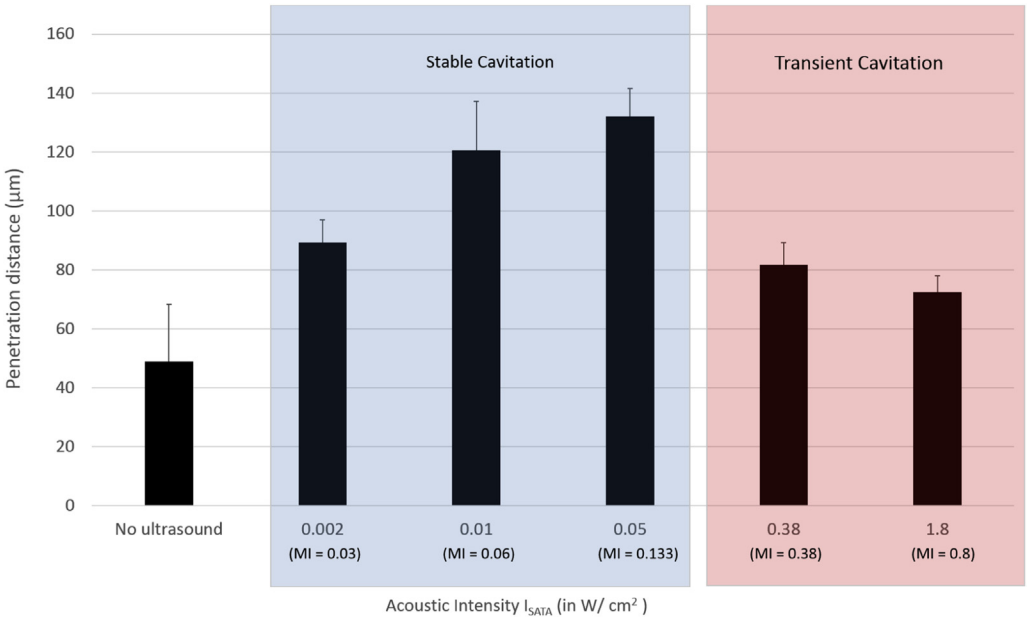

Fig. 4. Penetration distance of 0.1 wt% isothiocyanate-labeled bovine serum albumin after 30 s of ultrasound radiation at 40 kHz at different intensity values, followed by 15 min of immersion (n = 3). $p < 0.05$, ultrasound-treated groups compared with control group. MI = mechanical index.

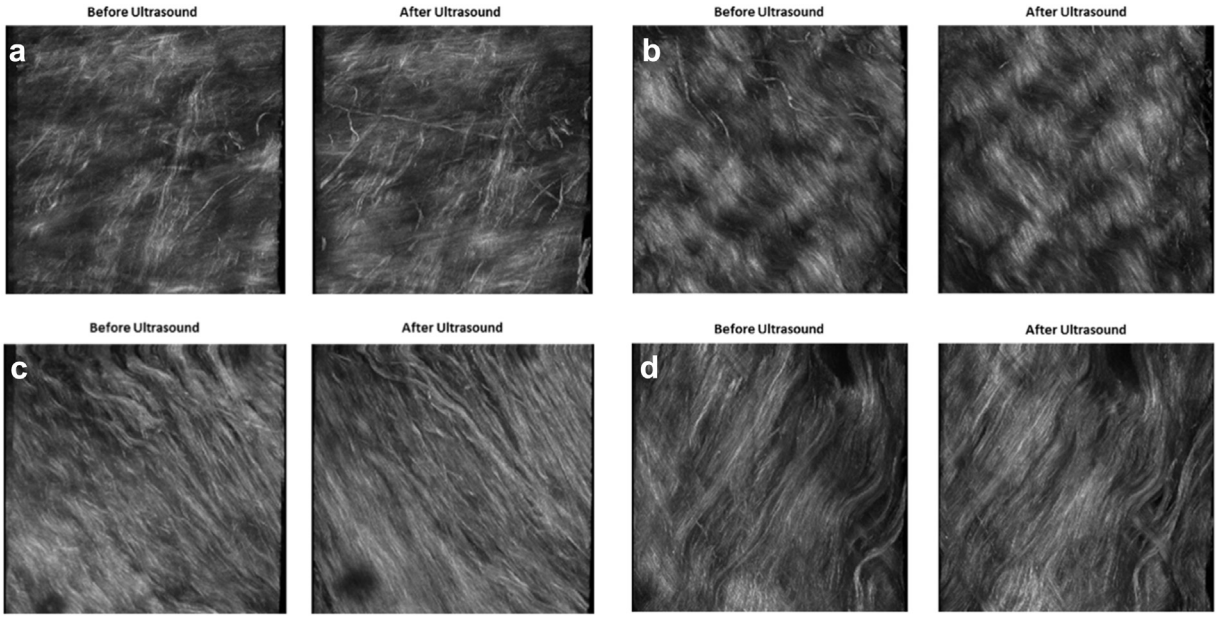

Fig. 5. Projection images: (a) I_{SATA} = 0.002 W/cm^2; (b) I_{SATA} = 0.05 W/cm^2; (c) I_{SATA} = 0.12 W/cm^2; (d) I_{SATA} = 1.8 W/cm^2. This imaging area measured 200 × 200 μm, 256 × 256 pixels.

at I_{SATA} = 0.0002, 0.05 and 0.12 W/cm^2. The temperature on the scleral surface increased 1.02 ± 0.8°C after sonication at an intensity of 1.8 W/cm^2. The changes in the scleral surface temperature were comparable to the calculation results based on ultrasound energy input (see Supplementary Material, online only, available at http://dx.doi.org/10.1016/j.ultrasmedbio.2016.07.013).

From Figure 4, the enhancement of transscleral penetration of FITC-BSA *ex vivo* was significantly higher in the low-intensity regime (I_{SATA} = 0.002, 0.01 and 0.05 W/cm^2) than in the high-intensity regime (I_{SATA} = 0.38 and 1.8 W/cm^2). Compared with control, 40-kHz ultrasound irradiation, regardless of the level of intensity, could significantly enhance the permeation of FITC-BSA along the transscleral route, with an increase from 48% to 63%. It is interesting to note that the increase in ultrasound intensity did not lead to a further increase in penetration distance of BSA along the transscleral route. Rather, the ultrasound intensity that leads to maximum penetration distance of BSA was observed only in the lower-intensity regime (I_{SATA} between 0.002 and 0.05 W/cm^2), which corresponds to the stable cavitation regime with the MI between 0.003 and 0.136.

Second harmonic generation imaging

Second harmonic generation images of the *ex vivo* sclera tissue were acquired by scanning the tissue from the outmost surface to the inner part, layer by layer. After scanning, the images obtained were stacked to generate Z-stack images before image projection to generate a 2-D image plane (Fig. 2). Figure 5 illustrates the typical projection images of *ex vivo* sclera tissue after ultrasound irradiation at I_{SATA} = 0.002, 0.05, 0.12 and 1.8 W/cm^2, respectively. Note that the same area of the sclera was imaged before and after ultrasound applications.

Image texture analysis

The final results of texture analysis are illustrated in Figure 6. The *t*-test reveals that the difference between the "control group" and all "treated groups" is not statistically significant ($p > 0.01$). Here, 1/entropy provides information on the density of collagen fibrils at a scale of 200 × 200 μm. *Ex vivo* sclera treated with 40 kHz at the ultrasound intensities tested did not exhibit significant changes in the 1/entropy value. Therefore, we can conclude that the overall interlacing pattern of collagen fibrils was not affected by 40-kHz ultrasound in both the low-intensity and high-intensity regimes. Because collagen fibril is reported to have a high level of anisotropy, fast Fourier transform analysis was conducted to capture the changes in anisotropy, that is, the dominant alignment direction of collagen fibrils in sclera after ultrasound irradiation. Again, *ex vivo* sclera tissue did not exhibit significant changes in collagen anisotropy on ultrasound irradiation at all tested intensities. Both entropy analysis and the asymmetric ratio of fast Fourier transform analysis were conducted on the entire image plane to provide information on the collagen interlacing pattern and collagen anisotropy at a macroscale (200 × 200 μm). On the contrary, GLCM correlation analysis focuses on the local correlation and variation of the collagen fibril pattern, which grasps the texture on a smaller scale

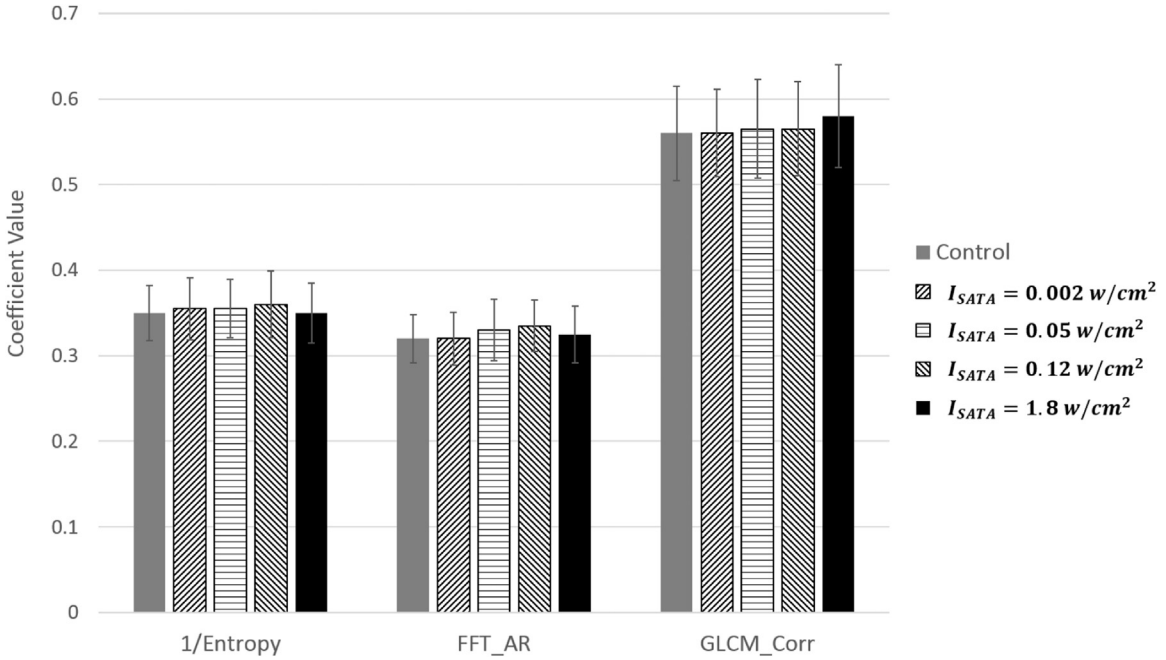

Fig. 6. Results of the texture analysis of the control (untreated sclera) and treated (ultrasound-exposed) groups. Results of the *t*-test indicate that the differences between the control and treated groups were not statistically significant. FFT_{AR} = asymmetric ratio of fast Fourier transform; GLCM = gray-level co-occurrence matrix; MI = mechanical index.

(20 × 20 μm). In this context, we are interested in evaluating if ultrasound irradiation would induce changes in the spacing, relative position and alignment direction of scleral collagen at a local level. From the mathematics perspective, collagen interlacing pattern and morphology (spacing, relative positions and alignment direction) were evaluated by first-order, second-order and higher-order statistical analyses, corresponding to entropy analysis, GLCM analysis and FFT_{AR}, respectively. Figure 6 illustrates that there were no observable changes in the collagen arrangement in both the low- and high-intensity regimes (I_{SATA} = 0.005, 0.05, 0.12 and 1.8 W/cm^2) from FFT_{AR} and GLCM analysis.

Intraocular pressure measurement

The typical intraocular pressure (IOP) e of untreated rabbit eye is 9.4 ± 0.4 mm Hg (Fig. 7). After 40-kHz ultrasound applications at the indicated intensities, the IOP value recorded after sonication did not change significantly ($p > 0.05$) compared with the IOP value recorded before sonication (Fig. 7).

Passive acoustic detection of cavitation

The presence of cavitation was verified by passive acoustic detection of bubble activity. Figure 8 illustrates the frequency spectra at 40 kHz at I_{SATA} = 0.05, 0.38 and 1.8 W/cm^2. Peaks at subharmonic (*f*/2) and fundamental (*f*) frequency, which denote the stable oscillation of bubbles, are present in the low-intensity regime (Fig. 8a). In the low-intensity regime (I_{SATA} = 0.05 W/cm^2), the distance between the fundamental and the noise floor was 54.44 dB (Fig. 8a). The distance between the fundamental and the noise floor decreased from 62.69 to 59.5 dB after ultrasound intensity increased from 0.38 to 1.8 W/cm^2 (Fig. 8b, c). This indicated the presence of inertial cavitation in the higher-intensity regime (Leighton 1994, 1995, 1997).

DISCUSSION

Herein, we have reported that low-frequency ultrasound did not induce changes in the collagen network

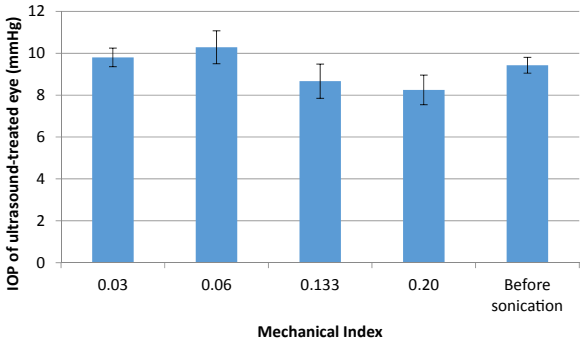

Fig. 7. Intraocular pressure (IOP) measurement of rabbit eye before and after 40-kHz ultrasound application at MI = 0.03–0.20. N = 5. There were no statistically significant differences ($p > 0.05$) between the ultrasound-exposed groups (MI = 0.03–0.20) and the control group.

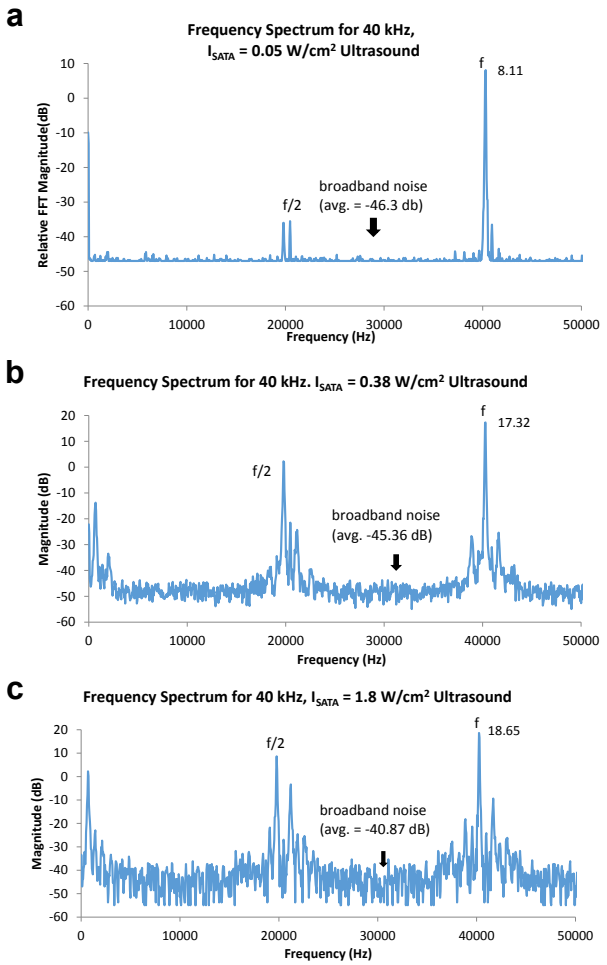

Fig. 8. Frequency spectrum for 40-kHz ultrasound at (a) I_{SATA} = 0.05 W/cm^2, (b) I_{SATA} = 0.38 W/cm^2, and (c) I_{SATA} = 1.8 W/cm^2. The "*f*" and "*f*/2" marks indicate the peak of the driving frequency and the subharmonic frequency. The presence of inertial cavitation at higher intensity regime was indicated by the reduction of the distance between the fundamental peak and the broadband noise. FFT = fast Fourier transform.

at all intensities tested, whereas transport of macromolecules along the transscleral route was significantly enhanced (Suen et al. 2013).

Rabbit sclera was chosen in this study to investigate the effect of ultrasound on scleral collagen arrangement. It has been reported that there is similar proteoglycan–collagen organization in human and rabbit sclera (Young 1985). It is interesting that the scleral collagen arrangement remained undisturbed after sonication at I_{SATA} values ranging from 0.002 to 1.8 W/cm^2. The presence of cavitation in the low-intensity regime appears to have had no effect on the scleral collagen matrix (Cheung et al. 2010). It is known that ultrasound can induce acoustic cavitation in which cavities alternately shrink and grow in size, oscillating in response to the subsequent high- and low-pressure portions of the ultrasound wave during stable cavitation (Merino et al. 2003). Stable cavitation occurs at low MIs (MI = 0.03–0.133, which is equivalent to I_{SATA} = 0.002–0.05 W/cm^2 in our setting), which is manifested by the periodic pulsation of bubbles or cavities in the medium. These pulsations create microstreaming, that is, fluid flow around the cavities (Hitchcock and Holland 2010; Soltani et al. 2008). Transient cavitation, on the other hand, is a vigorous form of cavity oscillations that results in violent collapse of the cavities. When this occurs, the bubble walls attain supersonic speeds on the collapse. When cavitations occur near or within the sclera, these microstreams could exert force on the collagen fibers. At the highest intensity tested (1.8 W/cm^2) in this study, however, the energy did not appear to induce any permanent changes in the collagen network.

The enhancement of the transscleral penetration of FITC-BSA *ex vivo*, interestingly, was higher in the stable cavitation regime (MI between 0.03 and 0.133, which is equivalent to I_{SATA} = 0.002–0.05 W/cm^2 in our setting). The enhancement of transscleral transport can be due to the microstreaming effects created by pulsating cavities in the medium during ultrasound application. The chaotic mixing induced by pulsating bubbles could enhance the permeation of macromolecules along the transscleral route. Though sufficient to induce microstreams that assist the permeation of FITC-BSA across the scleral tissue, the energy from stable cavitation did not produce changes in the collagen network. Because there are no guidelines on the use of ultrasound for delivery of ocular drugs, we benchmarked the ultrasound setting in our study to the U.S. Food and Drug Administration (USFDA) regulation for diagnostic imaging (USFDA 2008) that the MI of ultrasound should not exceed 0.23 for ophthalmic use (USFDA 2008). With respect to the ultrasound-induced heating effect, USFDA regulations require that the ultrasound system for ophthalmic use should have a thermal index <1. We observed negligible temperature changes on the scleral surface ($<1^\circ$C) at all acoustic outputs tested. The negligible changes in temperature on the scleral surface were supported by the low energy input by the ultrasound probe. Negligible temperate changes ($<0.1^\circ$C) were detected after the sclera was sonicated at I_{SATA} = 0.0002, 0.05 and 0.12 W/cm^2. The temperature on the scleral surface increased 1.02 ± 0.8°C after sonication at an intensity of 1.8 W/cm^2. The changes in scleral surface temperature were comparable to the results calculated on the basis of ultrasound energy input (see Supplementary Material). As we have shown that the enhancement by ultrasound in transscleral delivery is optimal under stable cavitation, maximum enhancement of delivery occurs without violating the current regulation.

The collagen fibril is a triple-helix molecular assembly that enables SHG imaging (Han et al. 2005). We adopted the two-photon excited fluorescence (TPEF)-SHG imaging technique to visually analyze the arrangement of collagen fibrils in the sclera before and after ultrasound applications. By taking advantage of the intrinsic properties of the collagen triple-helix arrangement, we could examine the collagen structure while minimizing artifacts caused by sample processing and labeling (Han et al. 2005). In our study, the aforementioned TPEF-SHG system can generate images with a resolution level that can distinguish between individual collagen fibrils and yield images for quantifying packing density in the formation of collagen bundles or lamellae (Denk et al. 1990).

Quantitative SHG image analysis techniques were employed to extract information on the collagen arrangement along the XY plane. Komai and Ushiki (1991) reported that collagen bundles or lamellae mostly run parallel to the XY plane, and therefore, it contains most of the features of the collagen network structure. Collagen fibrils in the sclera interweave with each other to form a network structure: the outer region consists of parallel-aligned collagen fibrils, which are packed into slender lamellae; increased interweaving of collagen fiber bundles replaces the lamellar arrangement in the deep sclera, with scattered elastic fibers throughout the stroma (Komai and Ushiki 1991). The overall texture randomness of collagen fibrils after ultrasound irradiation did not reveal significant changes as indicated by data from SHG image entropy analysis, which implies there is no thinning of collagen fibers. FFT analysis has been used to evaluate the orientation index (or anisotropy) of SHG images of skin and corneal collagen fibers, which is effective for discrimination of collagen fibers with and without a particular orientation (Hamanaka 1989; Matteini et al. 2009; Rayleigh 1879). From our results, collagen fibrils did not exhibit significant changes in alignment orientation after ultrasound irradiation at various MIs. To further differentiate morphologic patterns of collagen fibrils (linear, curved or disordered), we adopted orientation-dependent GLCM analysis. GLCM analysis revealed that there was insignificant change in the regularity and continuity of collagen bundles after ultrasound irradiation at both low intensity (I_{SATA} between 0.002 and 0.05 W/cm^2) and high intensity (I_{SATA} = 0.38 and 1.8 W/cm^2). These findings clearly indicate that ultrasound application in the low-intensity regime (with an equivalent MI from 0.03 to 0.20) and high-intensity regime (with an equivalent MI from 0.38 and 0.8) does not raise safety concerns, as scleral collagen remained unchanged. The elaborate intertwining nature of the collagen bundles is functionally important because this structure is considered to be effective in giving the eyeball its rigidity and flexibility against changes in intraocular pressure. Previous studies have reported that this scleral thinning is associated with a narrowing and dissociation of the collagen fiber bundles and a reduction in collagen fibril diameter (Curtin et al. 1979). Changes in the biochemical structure of the sclera, such as altered glycosaminoglycan (GAG) and collagen content (Avetisov et al. 1983), have also been reported in highly myopic postmortem human eyes and are further evidence of scleral pathology in high myopia. In our study, we did not observe changes from the scleral collagen arrangement; thus, ultrasound application for enhanced transscleral transport is a safe approach for delivery of ocular drugs.

In addition to the texture analysis of SHG images, the results of IOP measurements further supported the notion that ultrasound application at the intensities tested did not alter scleral structure. It is known that changes in IOP indicate that the mechanical property of the sclera is altered (Palko et al. 2011). No significant changes in intraocular pressure were observed, and thus, we concluded that ultrasound did not induce changes in the mechanical properties of the sclera before and after treatment.

This finding further indicates that cavitation activity-induced sonication in the low-MI regime (MI = 0.03–0.20, stable cavitation) and high-MI regime (MI = 0.38–0.8, transient cavitation) would not affect scleral collagen structure. Cavitation is the formation or interaction of cavities in the liquid body caused by rapid changes in pressure; often the cavities formed in the lower-pressure regions of the liquid. Effects of cavitation can be measured using the MI (Holland and Apfel 1989). The MI is the ratio between peak negative pressures generated by the ultrasound and the frequency. When low-frequency, low-intensity ultrasound radiated on the sclera in the presence of a liquid medium, cavitation occurred. In the stable cavitation regime, cavities in the medium started to pulsate periodically without violent collapse. From the results of passive cavitation detection, our ultrasound system could trigger stable cavitation when ultrasound was generated at I_{SATA} between 0.002 and 0.12 W/cm^2. When ultrasound intensity increased to 0.38 W/cm^2, cavities in the medium started to pulsate vigorously and eventually burst; the bubble walls attained supersonic speeds and created microjets (Apfel and Holland 1991). This phenomenon was observed in our ultrasound system at I_{SATA} = 0.38 and 1.8 W/cm^2, validated by the reduction in distance between the broadband noise and the fundamental signal. (Leighton 1997).

In combining the results of protein transscleral penetration with SHG imaging analysis, it is interesting to note that enhanced permeation of macromolecules across the sclera could be achieved by cavitation, at low MI,

without upsetting the scleral collagen arrangement. The study confirms that changes in the scleral collagen network are not necessary for transscleral penetration enhancement. This is desirable for future ultrasound-mediated transscleral delivery of therapeutics to the eye because of the strategic location and function of the sclera as the outermost barrier and mechanical support of the eyeball.

As mentioned in the previous section, the sclera is composed of collagen fibrils interlinked with proteoglycan molecules. A thorough analysis of the effect of ultrasound on the scleral collagen network was carried out and reported in previous sections. However, little is known about the effect of ultrasound on non-collagen constituents. Further studies on non-collagen constituents are required to have a better understanding of the enhanced transscleral penetration of macromolecules observed in previous study.

CONCLUSIONS

Penetration of macromolecules to the sclera is enhanced by ultrasound, and no permanent changes in the scleral collagen network are observed. Optimal transscleral transport enhancement lies within the low-intensity regime. We conclude that low-frequency, low-intensity ultrasound does not affect the scleral collagen fibrillar interlacing pattern and anisotropy. A systematic study was conducted to evaluate the effect of ultrasound on collagen fibril arrangement. The results from quantitative image analysis revealed that the differences in the collagen fibril arrangement after application of 40-kHz continuous ultrasound to *ex vivo* sclera tissue in both the low-intensity and high-intensity regimes were not significant.

Acknowledgments—The research work was supported by Hong Kong University Grant Committee—Research Infrastructure Grant FSGRF14 EG09.

SUPPLEMENTARY DATA

Supplementary data related to this article can be found at http://dx.doi.org/10.1016/j.ultrasmedbio.2016.07.013.

REFERENCES

Ambati J, Adamis AP. Transscleral drug delivery to the retina and choroid. Prog Retinal Eye Res 2002;21:145–151.
Ambati J, Gragoudas ES, Miller JW, You TT, Miyamoto K, Delori FC, Adamis AP. Transscleral delivery of bioactive protein to the choroid and retina. Invest Ophthalmol Visual Sci 2000;41:1186–1191.
Apfel RE, Holland CK. Gauging the likelihood of cavitation from short-pulse, low-duty cycle diagnostic ultrasound. Ultrasound Med Biol 1991;17:179–185.
Avetisov ES, Savitskaya NF, Vinetskaya MI, Iomdina EN. A study of biochemical and biomechanical qualities of normal and myopic eye sclera in humans of different age groups. Metab Pediatr Syst Ophthalmol 1983;7:183–188.
Cheung AC, Yu Y, Tay D, Wong HS, Ellis-Behnke R, Chau Y. Ultrasound-enhanced intrascleral delivery of protein. Int J Pharm 2010;401:16–24.
Chopra P, Hao J, Li SK. Iontophoretic transport of charged macromolecules across human sclera. Int J Pharm 2010;388:107–113.
Curtin BJ, Iwamoto T, Renaldo DP. Normal and staphylomatous sclera of high myopia: An electron microscopic study. Arch Ophthalmol 1979;97:912–915.
Denk W, Strickler JH, Webb WW. Two-photon laser scanning fluorescence microscopy. Science 1990;248:73–76.
Ethier CR, Johnson M, Ruberti J. Ocular biomechanics and biotransport. Ann Rev Biomed Eng 2004;6:249–273.
Farny CH, Holt RG, Roy RA. Temporal and spatial detection of HIFU-induced inertial and hot-vapor cavitation with a diagnostic ultrasound system. Ultrasound Med Biol 2009;35:603–615.
Ferguson JR. Using the grey-level co-occurrence matrix to segment and classify radar imagery. Reno, Ann Arbor, MI: ProQuest; 2007. p. 174.
Fine S, Hansen WP. Optical second harmonic generation in biological systems. Appl Opt 1971;10:2350–2353.
Geroski DH, Edelhauser HF. Transscleral drug delivery for posterior segment disease. Adv Drug Deliv Rev 2001;52:37–48.
Hamanaka T. Scleral spur and ciliary muscle in man and monkey. Jpn J Pphthalmol 1989;33:221–236.
Han M, Giese G, Bille J. Second harmonic generation imaging of collagen fibrils in cornea and sclera. Opt Express 2005;13:5791–5797.
Haralick RM. Statistical and structural approaches to textures. Proc IEEE 1979;67:786–804.
Hitchcock KE, Holland CK. Ultrasound-assisted thrombolysis for stroke therapy: Better thrombus break-up with bubbles. Stroke 2010;41:S50–S53.
Holland CK, Apfel RE. An improved theory for the prediction of microcavitation thresholds. IEEE Trans Ultrason Ferroelectr Freq Control 1989;36:204–208.
Ihara S. Information theory for continuous system. Singapore: World Scientific; 1993.
Kim SH, Lutz RJ, Wang NS, Robinson MR. Transport barriers in transscleral drug delivery for retinal diseases. Ophthalmic Res 2007;39:244–254.
Komai Y, Ushiki T. The three-dimensional organization of collagen fibrils in the human cornea and sclera. Invest Ophthalmol Visual Sci 1991;32:2244–2258.
Kuczynski K, Mikolajczak P. Information theory based medical images processing. Opto-Electron Rev 2003;11:253–259.
Leighton TG. Acoustic bubble detection: 1. The detection of stable gas bodies. Environ Eng 1994;9–16.
Leighton TG. Acoustic bubble detection: 2. The detection of transient cavitation. Environ Eng 1995;17–25.
Leighton TG. The acoustic bubble. New York/London: Academic Press; 1997.
Lim KS, Wickremasinghe SS, Cordeiro MF, Bunce C, Khaw PT. Accuracy of intraocular pressure measurements in new zealand white rabbits. Invest Ophthalmol Visual Sci 2005;46:2419–2423.
Matteini P, Ratto F, Rossi F, Cicchi R, Stringari C, Kapsokalyvas D, Pavone FS, Pini R. Photothermally-induced disordered patterns of corneal collagen revealed by SHG imaging. Opt Express 2009;17:4868–4878.
Merino G, Kalia YN, Guy RH. Ultrasound-enhanced transdermal transport. J Pharm Sci 2003;92:1125–1137.
National Council on Radiation Protection and Measurements (NCRP). Biological effects of ultrasound: Mechanisms and clinical implications. Bethesda, MD: Author; 1983.
Palko JR, Pan X, Liu J. Dynamic testing of regional viscoelastic behavior of canine sclera. Exp Eye Res 2011;93:825–832.
Rayleigh FRS. Investigations in optics, with special reference to the spectroscope. Philos Mag 1879;58:261–274.
Schmucker C, Ehlken C, Hansen LL, Antes G, Agostini HT, Lelgemann M. Intravitreal bevacizumab (Avastin) vs. ranibizumab

(Lucentis) for the treatment of age-related macular degeneration: A systematic review. Curr Opin Ophthalmol 2010;21:218–226.
Soltani A, Volz KR, Hansmann DR. Effect of modulated ultrasound parameters on ultrasound-induced thrombolysis. Phys Med Biol 2008; 53:6837–6847.
Suen WL, Wong HS, Yu Y, Lau LC, Lo AC, Chau Y. Ultrasound-mediated transscleral delivery of macromolecules to the posterior segment of rabbit eye in vivo. Invest Ophthalmol Visual Sci 2013; 54:4358–4365.
Szabo T. Diagnostic ultrasound imaging: Inside out. Orlando, FL: Academic Press; 2004.
Thrimawithana TR, Young SA, Bunt CR, Green CR, Alany RG. In-vitro and in-vivo evaluation of carrageenan/methylcellulose polymeric systems for transscleral delivery of macromolecules. Eur J Pharm Sci 2011;44:399–409.
U.S. Food and Drug Administration (USFDA). Guidance for industry and FDA staff: Information for manufacturers seeking marketing clearance of diagnostic ultrasound systems and transducers. Silver Spring, MD: Author; 2008.
Watson PG, Young RD. Scleral structure, organisation and disease: A review. Exp Eye Res 2004;78:609–623.
Young RD. Ultrastructural organization of proteoglycans and collagens in human and rabbit scleral matrix. J Cell Sci 1985;74:95–104.
Zeng Y, Yan B, Sun Q, He S, Jiang J, Wen Z, Qu JY. In vivo microvascular imaging and flow cytometry in zebrafish using two-photon excited endogenous fluorescence. Biomed Express 2014;5: 653–663.
Zheng W, Li D, Li S, Zeng Y, Yang Y, Qu JY. Diagnostic value of nonlinear optical signals from collagen matrix in the detection of epithelial precancer. Opt Lett 2011;36:3620–3622.